Nanoscale

PAPER

View Article Online
View Journal

Cite this: DOI: 10.1039/d6nr00946h

Template-assisted assembly of structurally diverse plasmonic nanoparticle chains

Jun-Hyun Kim, [a] Jung Young Jung,[b] Yonghyeon Kim, [b] Ui Jeong Pyo,[b] Yeji Han,[c] Seunghoon Lee, [d] Jong Wook Hong, [e] Dae Han Wi *[f] and Sang Woo Han *[b]

One-dimensional (1D) plasmonic nanoarchitectures have attracted substantial interest owing to their highly tunable plasmonic properties, optical responses to the long-wavelength region, and directional light propagation. However, fabricating finite 1D chains with diverse geometries remains challenging. Here, we report an anodic aluminum oxide (AAO) template-mediated strategy to assemble plasmonic metal nanoparticles (NPs) into 1D nanochains. By promoting the hydrophilicity of the AAO channels *via* H_2O_2 treatment, we achieved uniform and dense pore filling with metal NPs, which could then be isolated in high yield after template removal. The length of the 1D NP chains could be controlled by adjusting the pore depth of the AAO template. This method is applicable to plasmonic NP building blocks with diverse shapes, sizes, and compositions. The resulting 1D NP chains exhibited shape- and geometry-dependent plasmonic features. Furthermore, our approach can be extended to realize 1D peapod-like architectures consisting of a plasmonic 1D NP chain core encapsulated within a plasmonic metal shell. This work presents a facile and versatile route for engineering 1D plasmonic nanoarchitectures with programmable geometries and tailored optical functions.

Received 9th March 2026,
Accepted 16th April 2026

DOI: 10.1039/d6nr00946h

rsc.li/nanoscale

Introduction

Diverse strategies have been extensively explored to precisely control the architecture of nanoscale metal particles with distinct physical and chemical properties.[1–3] In particular, the assembly of optically active metal nanoparticles (NPs) into one-dimensional (1D) chains can render highly tunable surface plasmon resonances (SPRs) across a wide range of wavelengths covering the UV, visible, and near-infrared (NIR) regions.[4–8] In such 1D architectures, properly aligned NPs exhibit strong near-field coupling, which not only tailors the transverse and longitudinal plasmon modes but also enhances local electromagnetic fields in a highly geometry-dependent manner.[9,10] Owing to their directional optical responses and tunability, linear NP chains built from structurally diverse plasmonic building blocks are attractive for various applications, including biological sensors, plasmonic rulers, and surface-enhanced Raman scattering (SERS) platforms.[11–13]

The 1D architectures of metal NPs are typically fabricated *via* either soft- or hard-templated approaches.[12] The soft-templated assembly relies on programmed interparticle interactions enabled by controlled surface functionalization,[4,7–11,13] whereas the hard-templated routes use prefabricated 1D scaffolds (*e.g.*, cylindrical pores, channels, or fibers) to confine and guide NP organization into 1D structures.[14–17] In most cases, these strategies rely on tailored surface modifiers, such as functional organic, biological, and polymeric ligands, to regulate colloidal interactions and direct NP organization in solution, where the resulting structures are typically governed by thermodynamic equilibria and free-energy minimization. Although considerable efforts have been devoted to modulating these thermodynamic forces to access non-equilibrium architectures, further advances are still needed to reduce experimental complexity and minimize the number of variables and processing steps. Moreover, even after aligned assemblies are established, achieving high-yield isolation of discrete, finite NP chains remains challenging, thereby impeding precise analysis of structure–property correlations. In this context, establishing a reliable and broadly applicable fabrication strategy to organize structurally diverse plasmonic NPs

[a]*Department of Chemistry, Illinois State University, Normal, Illinois 61790-4160, USA*
[b]*Department of Chemistry, KAIST, Daejeon 34141, Korea. E-mail: sangwoohan@kaist.ac.kr*
[c]*Technical Support Center for Chemical Industry, Korean Research Institute of Chemical Technology (KRICT), Ulsan 44412, Korea*
[d]*Department of Chemistry and Department of Chemical Engineering (BK21 FOUR Graduate Program), Dong-A University, Busan 49315, Korea*
[e]*Department of Energy Engineering, Korea Institute of Energy Technology (KENTECH), Naju 58330, Korea*
[f]*Department of Chemistry, Chungnam National University, Daejeon 34134, Korea. E-mail: dhwi@cnu.ac.kr*

into well-defined 1D chains with high yield would enable the development of viable systems for elucidating structure-dependent optical properties, including light propagation and SPR characteristics.

Here, we present a strategy to fabricate controlled 1D nanochains of diverse plasmonic metal NPs in high yield using anodized aluminum oxide (AAO) templates. Among the diverse types of 1D channel templates, we chose AAO as a template due to its well-defined cylindrical pores and the facile tunability of its pore diameter and depth.[17–21] Most previous AAO-templated approaches for constructing 1D NP chains have employed metal NPs synthesized in organic media or polymer-encapsulated NPs dispersible in organic solvents for template infiltration.[17–21] However, this limits the accessible library of metal NP building blocks, as a wide variety of NPs with tunable shapes, sizes, and compositions are synthesized in the aqueous phase.[22–24] To enable efficient infiltration of aqueous colloidal plasmonic NPs into AAO pores and thereby form 1D NP chains without additional surface functionalization and extensive solvent screening, we rendered the AAO surface hydrophilic, achieving dense packing of NPs within the pores. The resulting 1D NP chains could be isolated in high yield through AAO template removal, thereby facilitating reliable optical characterization. For instance, we obtained 1D chains of Au nanospheres (NSs) with systematically varied lengths by simply adjusting the AAO pore depth and observed apparent length-dependent plasmonic features. Notably, because the diameter of the Au NSs is smaller than that of the AAO pores, a zigzag-like packing geometry can emerge, giving rise to an additional plasmonic feature. Our method can indeed be applicable to other metal NPs with diverse morphologies and compositions, allowing systematic investigation of the plasmonic behaviors of 1D NP chains depending on their NP building blocks and chain lengths. Furthermore, our strategy can be extended to generate peapod-like architectures *via* post-galvanic replacement of Au@Ag core–shell NP 1D chains.

Results and discussion

For the fabrication of 1D plasmonic metal NP chains, AAO templates with a fixed pore diameter of 80 nm and varying pore depths (100, 200, 300, and 500 nm) were prepared through the anodization of Al foils.[17] Scanning electron microscopy (SEM) images of an AAO template with a pore depth of 500 nm are shown in Fig. S1. To achieve high-yield fabrication of well-defined 1D NP chains, we optimized the process using Au NSs with an average diameter of 55 ± 5 nm (Fig. S2a). Scheme 1 depicts the overall AAO-templated fabrication procedure for Au NS 1D chains. Briefly, the AAO template was treated with H_2O_2 to enhance surface hydrophilicity, followed by loading of a concentrated aqueous Au NS colloidal solution onto the AAO surface under vacuum. Capillary forces during solvent evaporation drove the Au NSs into the AAO channels, enabling dense packing within the pores. The pore-filled NS assembly was subsequently treated with a linker

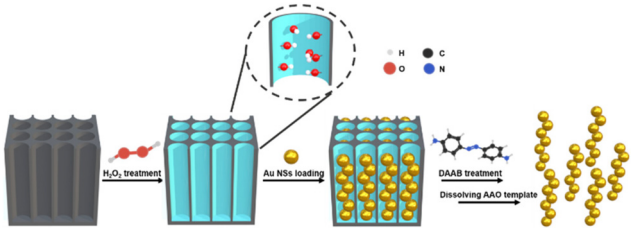

Scheme 1 Schematic illustration of the fabrication of Au NS 1D chains using AAO templates.

molecule, 4,4′-diaminoazobenzene (DAAB), which plays a pivotal role in reinforcing the structural integrity of the chains. Finally, the AAO template was dissolved in phosphoric acid to release the Au NS 1D chains.

For the efficient infiltration of aqueous colloidal Au NSs into the AAO pores, we treated the AAO template with H_2O_2 to render the AAO surface more hydrophilic. To verify that the H_2O_2 treatment enhances the surface hydrophilicity of the AAO template, the contact angle of a water droplet on the AAO template was measured before and after the treatment, indicating that the contact angle decreased markedly from ≥65° to ≤45° after the treatment (Fig. 1a). This enhanced wettability is attributed to the higher surface density of hydroxyl groups gen-

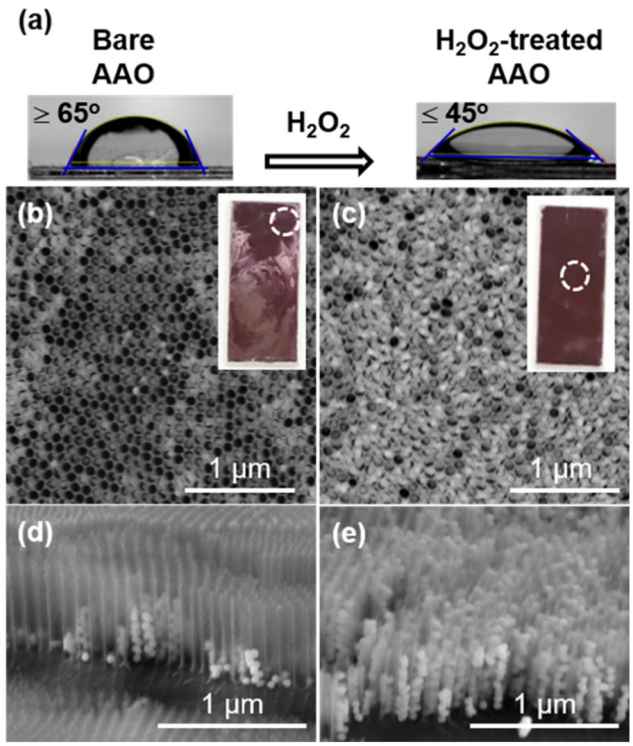

Fig. 1 (a) Water contact angles of the AAO surface before and after the H_2O_2 treatment. SEM (b and c) top- and (d and e) side-view images of Au NS-loaded (b and d) bare AAO and (c and e) H_2O_2-treated AAO templates. The insets in panels b and c show the photographs of the Au NS-loaded AAO templates, in which the areas used for the SEM measurements are indicated with dashed circles.

erated on the AAO surface upon H_2O_2 treatment.[25,26] To demonstrate the effect of H_2O_2 treatment on pore filling, bare AAO and H_2O_2-treated AAO templates were compared after loading an aqueous Au NS colloidal solution (Fig. 1b–e). Notably, the use of a bare AAO template without H_2O_2 treatment resulted in relatively poor adsorption of the Au NSs on the template surface, making it difficult to achieve reproducible packing. Even after the multiple loading steps, the surface of the untreated AAO template displayed an irregular color distribution, indicating uneven packing of the Au NSs (inset of Fig. 1b). In stark contrast, the H_2O_2-treated AAO template exhibited an evenly distributed red coloration after Au NS loading (inset of Fig. 1c), suggesting substantially improved packing uniformity. The SEM images of the top surfaces and cross-sections of the Au NS-loaded AAO templates further confirm the difference in packing efficiency. The Au NSs densely and uniformly filled the H_2O_2-treated AAO pores (Fig. 1c and e), whereas incomplete and nonuniform pore filling of the Au NSs was observed in the untreated AAO template even when the surface appeared red (Fig. 1b and d). Collectively, incorporating a simple H_2O_2 treatment enables the reliable preparation of Au NS 1D chains while bypassing the need for solvent exchange and/or complex surface modifications otherwise required prior to NP assembly.[15,17–21] Upon complete pore filling and surface cleaning, the Au NS-filled AAO template was treated with the DAAB linker to reinforce and preserve the assembled 1D chain structure. The template was subsequently dissolved in phosphoric acid to isolate the Au NS 1D chains.

With the optimized fabrication conditions, Au NS 1D chains with controlled chain lengths were produced using AAO templates with varying pore depths. After template removal, the released Au NS 1D chains were obtained as a colloidal dispersion, which enabled subsequent microscopic and spectroscopic characterization. Fig. 2 shows the representative SEM and transmission electron microscopy (TEM) images of the prepared Au NS 1D chains and the corresponding UV-vis-NIR extinction spectra. The distributions of chain lengths and the number of constituent Au NSs in the Au NS 1D chains are shown in the insets of Fig. 2a–d and Fig. S3, respectively. The SEM images reveal that the Au NSs infiltrated into the AAO templates predominantly formed quasi-linear 1D chains, and the chain length and the number of constituent Au NSs increase as the AAO pore depth increases (Fig. 2a–d). The fraction of free particles was less than 2% in all cases, except for the Au NS 1D chains prepared using an AAO template with a pore depth of 100 nm, which exhibited a free particle fraction of approximately 20% (Fig. S3), demonstrating the high-yield production of 1D NP chains. Notably, with increasing chain length, the packing geometry progressively transformed from a linear to a staggered configuration, giving rise to a zigzag-like chain morphology. Specifically, for the Au NS 1D chains prepared using an AAO template with a pore depth of 500 nm, the average zigzag angle was estimated to be 102 ± 21°. Consequently, the number of Au NSs per chain exceeded the value predicted for ideal linear packing at a given projected

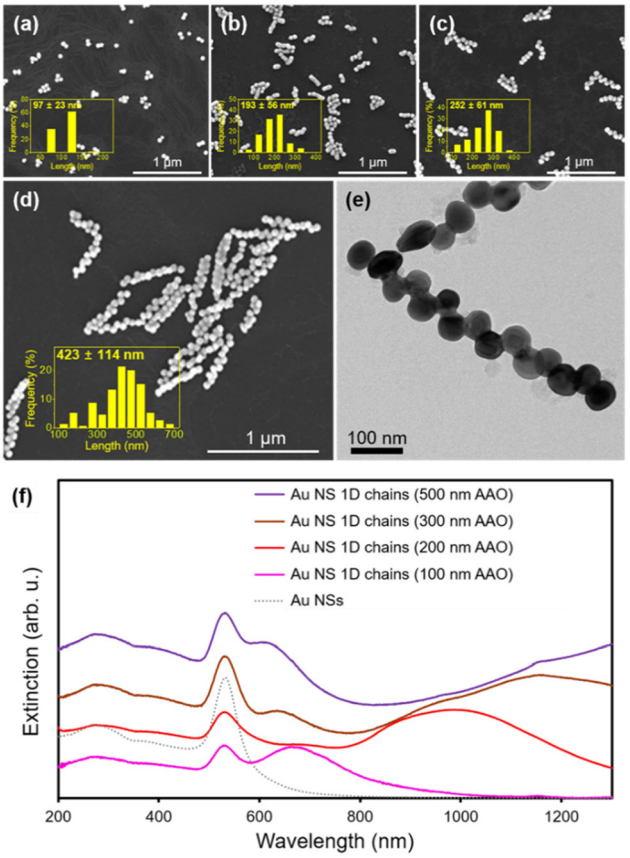

Fig. 2 SEM images of Au NS 1D chains prepared using AAO templates with pore depths of (a) 100, (b) 200, (c) 300, and (d) 500 nm. The insets show the chain length distributions. (e) TEM image of Au NS 1D chains prepared using an AAO template with a pore depth of 500 nm. (f) UV-vis-NIR extinction spectra of the Au NS 1D chains and Au NSs.

chain length for the chains with a zigzag-like morphology. For instance, a substantial fraction of the Au NS 1D chains with an average projected length of 423 nm contained 11–14 NSs, significantly exceeding the ~8 NSs predicted for ideal linear packing (Fig. 2d and Fig. S3d). In contrast, the majority of Au NS 1D chains with an average projected length of 193 nm accommodated 3–4 NSs, consistent with the value expected for a linear configuration (Fig. 2b and Fig. S3b). Given that the pore diameter is substantially larger than the diameter of the Au NSs, the lateral free space between the pore wall and the NS surface allows adjacent NSs to adopt a staggered packing configuration. As the number of Au NSs increases, this staggered packing can propagate along the chain, leading to a zigzag-like assembly and, hence, effectively increasing the number of coupled NSs per chain. TEM analysis further confirmed that most adjacent NSs are in intimate contact with no discernible interparticle gaps, with certain NSs even undergoing partial coalescence (Fig. 2e). The intimate contact between NSs is likely caused by capillary force-driven compaction during pore filling. Although intimate contact and partial coalescence between NSs can help maintain interparticle connectivity and preserve the chain structure, the Au NS-loaded AAO templates

were further treated with the DAAB linker overnight to reinforce the chain integrity before template dissolution, as we mentioned above. Indeed, bifunctional molecules, like DAAB, have been employed as effective NP cross-linkers for the controlled assembly of NPs.[27] Notably, Au NS chains prepared without the linker treatment fragmented into substantially shorter segments compared to those prepared with the linker (Fig. S4), implying that the interparticle contact between adjacent Au NSs is not fully persistent along the entire chain. Accordingly, bridging the interparticle junctions with the DAAB linker is required to preserve chain integrity and thus obtain intact 1D chains upon template dissolution.

As shown in Fig. 2f, whereas the Au NSs exhibit a single SPR peak at 530 nm, the Au NS 1D chains display broad low-energy SPR peaks alongside the original Au NS SPR peak. The low-energy SPR peaks are significantly red-shifted from 670 to >1300 nm with increasing chain length, confirming that these peaks correspond to chain plasmon modes across the 1D structure.[28–30] The spectral region beyond 1300 nm is not readily accessible for extinction measurements in the aqueous phase owing to the strong infrared absorption of water. These spectral features indicate that the majority of the Au NSs were assembled into well-defined 1D chains using our template-assisted approach, rather than forming disordered aggregates. In addition, partial coalescence between adjacent Au NSs may also influence the optical response by facilitating more extended plasmonic coupling along the chain.[28] Hereafter, the Au NS SPR peak and the chain plasmon mode peak are referred to as the transverse and longitudinal SPR peaks, respectively. Interestingly, additional shoulder peaks are evident in the 600–700 nm spectral region for the Au NS chains exceeding 200 nm in length. Given that the Au NS chains deviate from a perfectly linear geometry and adopt a staggered (zigzag-like) configuration, an additional plasmon mode is expected to emerge from the bent chain segments, likely accounting for the observed shoulder peak.[30,31] Consistent with this interpretation, the shoulder feature intensifies as the staggered alignment becomes more pronounced with increasing chain length. To further verify that the zigzag packing is responsible for the shoulder peaks, large Au NSs with an average diameter of 71 ± 5 nm (Fig. S2b) were assembled into 1D chains using AAO templates with pore depths of 300 and 500 nm (Fig. S5a and b). In contrast to the standard Au NSs, the larger Au NSs formed 1D chains with an almost linear morphology, likely because the reduced free space within the pores constrains lateral displacement. Apparently, the significant reduction in the zigzag configuration of the formed 1D chains led to the disappearance of the shoulder peaks (Fig. S5c), supporting our inference that the shoulder peak originates from the zigzag packing of the Au NSs within the 1D arrangement.

To better understand the SPR features of the Au NS 1D chains, finite-difference time-domain (FDTD) simulations were performed using a model 1D zigzag chain (length = 450 nm, number of NSs = 12) representative of the Au NS 1D chains assembled within an AAO template with a pore depth of

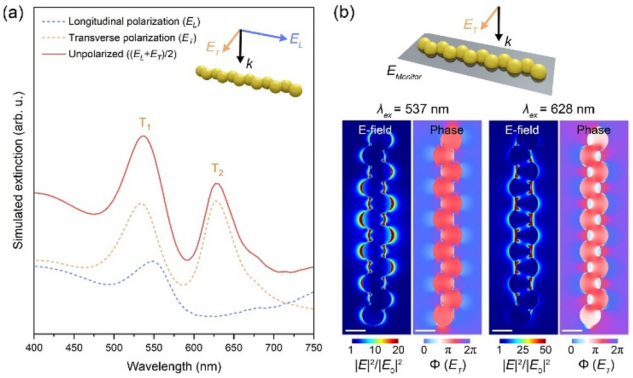

Fig. 3 (a) Simulated extinction spectrum of a model Au NS 1D zigzag chain shown in the inset (length = 450 nm, number of NSs = 12). (b) Electric field intensity ($|E|^2/|E_0|^2$) and phase (Φ) distributions of the model Au NS 1D zigzag chain shown through a monitor plane ($E_{Monitor}$) at the excitation wavelengths (λ_{ex}) of 537 and 628 nm, which correspond to the T_1 and T_2 modes, respectively. Scale bars indicate 50 nm.

500 nm (inset of Fig. 3a). As shown in the simulated extinction spectrum of the model 1D chain in the transverse-mode region, a typical transverse resonance (T_1 mode) is observed at 537 nm (Fig. 3a). Notably, an additional peak emerges at 628 nm, adjacent to the T_1 mode peak. This feature is assigned as a secondary transverse mode, T_2 mode, likely corresponding to the shoulder peak observed in the experimental extinction spectrum. To elucidate the origin of this mode, we analyzed the resonant electric field intensity ($|E|^2/|E_0|^2$) and phase (Φ) distributions of the different plasmon modes (Fig. 3b). While the T_1 mode is characterized by vertical electric field oscillations localized on individual Au NSs, the T_2 mode exhibits strong electric fields concentrated between adjacent NSs, which can be attributed to the near-field coupling between NSs rendered by the zigzag geometry. The corresponding phase map also shows in-phase near-field coupling between neighboring NSs. These simulation results confirm that the bent chain segments arising from the zigzag packing geometry enable a new plasmon coupling mode, the T_2 mode.[17,31] Since the prepared Au NS zigzag 1D chains exhibit broad chain-length distributions, such ensemble heterogeneity may influence the spectral features. To investigate this potential influence, additional FDTD simulations were conducted for model Au NS zigzag chains with different chain lengths (Fig. S6). Notably, the simulated transverse-mode features, including the T_2 mode-related shoulder, remained consistent despite variations in chain length. This is likely because the transverse mode is much less sensitive to chain-length variation when the lateral dimensions remain unchanged, in contrast to the longitudinal mode, which strongly depends on the overall chain length. These results indicate that ensemble heterogeneity has little effect on the spectral features.

The present method can be readily extended to fabricate 1D chains of Au NPs with diverse morphologies. Fig. 4 presents the SEM and TEM images of 1D chains with varying lengths assembled from Au nanocubes (NCs, Fig. S2c) with an average

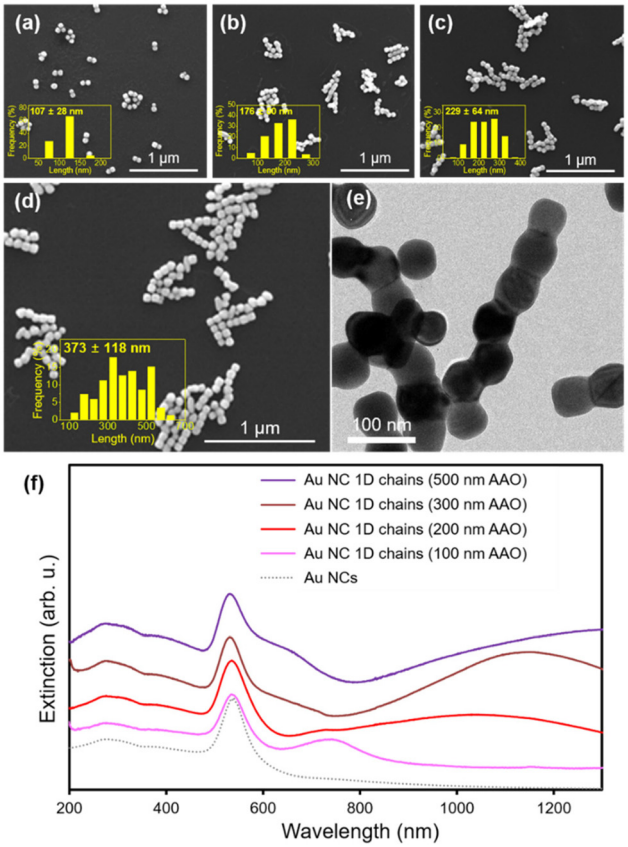

Fig. 4 SEM images of Au NC 1D chains prepared using AAO templates with pore depths of (a) 100, (b) 200, (c) 300, and (d) 500 nm. The insets show the chain length distributions. (e) TEM image of Au NC 1D chains prepared using an AAO template with a pore depth of 500 nm. (f) UV-vis-NIR extinction spectra of the Au NC 1D chains and Au NCs.

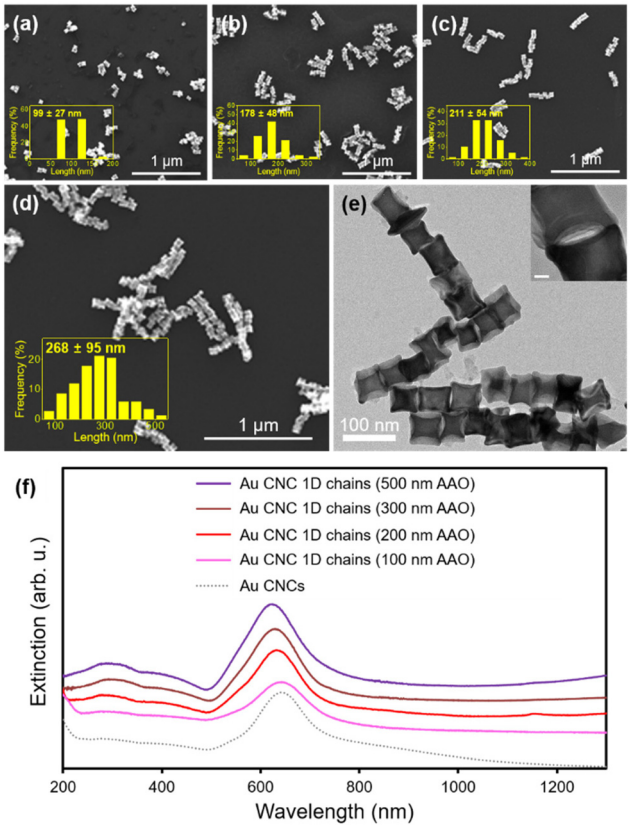

Fig. 5 SEM images of Au CNC 1D chains prepared using AAO templates with pore depths of (a) 100, (b) 200, (c) 300, and (d) 500 nm. The insets show the chain length distributions. (e) TEM image of Au CNC 1D chains prepared using an AAO template with a pore depth of 500 nm. The inset shows a high-magnification TEM image of an interparticle region (scale bar = 10 nm). (f) UV-vis-NIR extinction spectra of the Au CNC 1D chains and Au CNCs.

size (57 ± 5 nm) comparable to that of the Au NSs, along with the corresponding UV-vis-NIR extinction spectra. Similar to the Au NSs, the Au NCs were arranged into 1D chains, of which the length and the number of constituent NCs increase as the AAO pore depth increases. However, the Au NC 1D chains are shorter and contain fewer NPs than the NS 1D chains, and the zigzag-like packing motif was less pronounced (Fig. 4a–e and Fig. S7). This is likely due to the larger interparticle contact area of the Au NCs compared to that of the Au NSs, which suppresses the misaligned arrangements. The Au NC 1D chains also exhibited two distinctive SPR peaks corresponding to the longitudinal and transverse modes, where the longitudinal peaks were gradually red shifted as the chain length increased (Fig. 4f). Spectral features associated with the T_2 mode were observed for the Au NC 1D chains exceeding 200 nm in length, although the peak intensities were considerably weaker than those of the NS chains. The reduced intensity of the T_2 mode can be attributed to the relatively straighter packing of the Au NC building blocks.

Meanwhile, concave NPs could also be assembled into 1D chains with the present method. Fig. 5 displays the microscopic images of 1D chains prepared with Au concave nanocubes (CNCs; average size: 55 ± 5 nm, Fig. S2d) and their corresponding UV-vis-NIR extinction spectra. As shown in Fig. 5a–d, the Au CNCs were well arranged into 1D chains with varying lengths as a function of the AAO pore depth. However, the Au CNC 1D chains adopt a straighter linear geometry with decreased chain lengths and the number of NPs per chain compared to the Au NS and NC 1D chains (Fig. 5a–d and Fig. S8). These morphological characteristics of the Au CNC 1D chains are also reflected in their UV-vis-NIR extinction spectra, in which no discernible T_2 mode peak is observed (Fig. 5f). Since the Au CNCs contain multiple high-curvature sites (*e.g.*, sharp vertices and edges), they preferentially adopt a face-on alignment rather than a diagonally tilted configuration within the confined AAO pores to maximize interparticle contact area. The resulting constraints on rotational and lateral degrees of freedom suppress the formation of a zigzag-like packing geometry. In addition, no distinct longitudinal mode peak is evident in the extinction spectra of the Au CNC 1D chains, suggesting that the longitudinal resonance likely resides beyond the accessible spectral range of aqueous-phase extinction measurements. This is attributed to the substan-

tially lower plasmon resonance energy of the Au CNCs relative to the other NP morphologies, arising from their locally thinned edges.[32,33] Another notable structural feature of the Au CNC 1D chains is the presence of curved interfacial gaps between neighboring particles (Fig. 5e). Through the synergistic combination of longitudinal plasmon resonance expected in the NIR region and well-defined interparticle nanogaps, the Au CNC 1D chains can be utilized as promising platforms for NIR-responsive plasmonic applications.[33–35]

Beyond the Au NPs shown above, our method can enable the formation of 1D assemblies from a wide range of plasmonic NPs with diverse sizes, morphologies, and compositions. For example, small Au NSs with an average diameter of 25 ± 2 nm (Fig. S2e) assembled into a cylinder-like structure, in which the cross-section comprised multiple (4–6) coalesced NSs (Fig. 6a). Meanwhile, Au bipyramids with average short- and long-axis lengths of 31 ± 5 and 90 ± 9 nm, respectively (Fig. S2f), formed 1D assemblies with discernible interparticle nanogaps (Fig. 6b). Moreover, 1D NP chains can also be prepared from binary plasmonic NPs, such as Au@Ag core–shell nanooctahedra (NOs; average size: 49 ± 4 nm, Fig. S2g) (Fig. 6c).

To further demonstrate the versatility of our approach for constructing novel nanoarchitectures, we note that AAO-assisted assembly has been previously employed to produce 1D Au NP assemblies with peapod-like architectures, in which an NP chain is encapsulated within a shell structure.[17,20] In most reported approaches, the shell comprises dielectric materials, such as SiO_2, which inherently limit plasmonic enhancement. Given that particle-in-a-frame or particle-in-a-shell nanostructures can be generated *via* the galvanic replacement of Au@Ag core–shell NPs,[24] we infer that the present method can allow the creation of a new class of plasmonic nanostructures, in which a plasmonic 1D chain core is encapsulated within a plasmonic shell. Indeed, we could fabricate a plasmonic peapod structure consisting of an Au NO 1D chain core encapsulated within an AuAg shell through the galvanic replacement of the Au@Ag NO 1D chains (Fig. 7). This architecture is expected to generate strong plasmonic coupling not only between adjacent Au NOs but also between the core and the surrounding shell, thereby rendering it highly promising for plasmonic sensing applications. To further support our claim, we performed additional optical characterization studies and FDTD simulations to examine the plasmonic properties of the peapod structures. The UV-vis-NIR extinction spectrum of the Au NO–AuAg peapod structures displays a broad plasmonic response extending from the visible to the NIR region (Fig. S9a). Furthermore, the FDTD-simulated $|E|^2/|E_0|^2$ distribution of a model Au NO–AuAg peapod structure reveals the formation of multiple hot spots within the peapod architecture, arising from plasmonic coupling between adjacent Au NOs and between the core chain and the surrounding shell (Fig. S9b). Notably, the prepared peapod structures could enable single-particle SERS detection of 4-methylbenzenethiol (4-MBT) under 633 nm laser excitation (Fig. S9c and d), distinctly corroborating their potential for plasmonic applications.

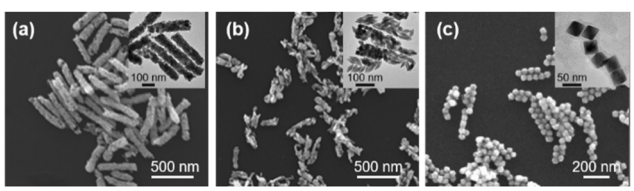

Fig. 6 SEM and TEM (inset) images of (a) small Au NS, (b) Au bipyramid, and (c) Au@Ag core–shell NO 1D chains prepared using AAO templates with a pore depth of 500 nm.

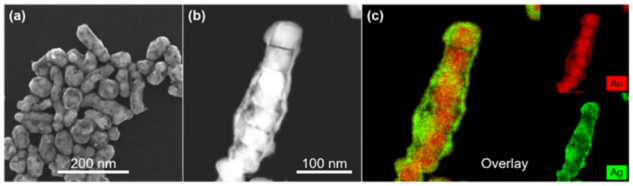

Fig. 7 (a) SEM, (b) high-angle annular dark-field scanning TEM (HAADF-STEM), and (c) corresponding energy-dispersive X-ray spectroscopy (EDS) elemental mapping images of Au NO–AuAg peapod nanostructures.

Conclusions

We have developed an AAO-templated strategy to fabricate controlled 1D chains of diverse plasmonic metal NPs. Promoting the hydrophilicity of AAO templates *via* H_2O_2 treatment substantially improved the uniformity and packing density of metal NPs within the AAO pores. We could then successfully isolate 1D NP chains in high yield through AAO template removal. Our strategy can be applicable to plasmonic Au NP building blocks with diverse shapes, sizes, and compositions and can further be extended to construct plasmonic 1D peapod-like nanoarchitectures. We envision that the present approach can serve as a versatile platform for engineering plasmonic 1D architectures with tunable chain lengths and confinement-dependent morphologies, thereby offering new opportunities to explore unconventional plasmonic functions and to advance the development of functional materials for diverse plasmonic applications.

Experimental

Materials

Al foil (99.99%, 0.25 mm thick, 100 × 500 mm^2, Alfa Aesar 40761), phosphoric acid (85.9%, J. T. Baker), ethanol (J. T. Baker), $HClO_4$ (70%, OCI Company Ltd), chromium(VI) oxide (Kanto Chemical), oxalic acid (99+%, Acros Organics), H_2O_2 (30%, Daejung Chemicals & Metals Co.), L-ascorbic acid (AA, 99.5%, Daejung Chemicals & Metals Co.), DAAB (95%, Alfa Aesar), $HAuCl_4{\cdot}3H_2O$ (>99.9%, Sigma-Aldrich), $AgNO_3$ (>99%, Sigma-Aldrich), cetyltrimethylammonium chloride

(CTAC, a solution in water, 25 wt%, Sigma-Aldrich), $NaBH_4$ (>98.0%, Sigma-Aldrich), KI (99%, Sigma-Aldrich), NaBr (≥99%, Sigma-Aldrich), HCl (37%, Sigma-Aldrich), 4-MBT (98%, Sigma-Aldrich), and ammonia solution (28.0–30.0% assay, Junsei Chemical) were used as received. Deionized water with a resistivity higher than 18.0 MΩ cm was used to prepare aqueous solutions.

Preparation of AAO templates

AAO templates with different pore depths were prepared by following a previously reported procedure with slight modifications.[17] A two-electrode setup with an Al foil and a stainless-steel plate as the working and counter electrodes, respectively, was used for the electropolishing and anodization steps. In a typical preparation of an AAO template, an Al foil (*ca.* 3 × 10 cm^2), cleaned with copious amounts of acetone, ethanol, and water, was immersed in an electropolishing solution (850 mL of ethanol + 150 mL of $HClO_4$) at 3.5 °C. The surface of the foil was gently blown with a pipette to prevent the deposition of brown debris during the polishing process. Then, the polished foil was soaked in an anodization solution (0.3 M oxalic acid; 37.8 g of oxalic acid in 1 L of water) at 8 °C for 8–10 h, in which the voltage was adjusted to 40 V and the current was set to 0.09–0.1 and 0.18 A for one and two Al foils, respectively. The anodized Al foil was etched using a mixture of phosphoric acid (41.57 mL) and 10% chromic acid (87.5 mL) at 60 °C for 3 h and then treated with the second anodization solution (fresh oxalic acid). Lastly, the Al foil was placed in a pore-widening solution (0.1 M phosphoric acid) in a water bath at 35 °C. The pore depth of the AAO templates was controlled by adjusting the durations of the second anodization and pore-widening processes: 1.5 and 5 min for 100 nm, 3 and 30 min for 200 nm, 5 and 35 min for 300 nm, and 7 and 45 min for 500 nm depths, respectively.

Synthesis of Au NPs with various shapes

To prepare Au NPs, Au NP seeds were synthesized first. In a typical synthesis of Au NP seeds, 0.6 mL of ice-cold 10 mM $NaBH_4$ was quickly injected into a thoroughly mixed solution of 10 mL of 100 mM CTAC and 0.5 mL of 5 mM $HAuCl_4{\cdot}3H_2O$. The reaction mixture was vigorously stirred for 1 min and stored at room temperature for 5 h before use. To prepare Au NSs, 0.03 mL of a 10-fold diluted Au NP seed solution was added to a mixture of 100 mM CTAC (20 mL), 5 mM $HAuCl_4{\cdot}3H_2O$ (4 mL), and 300 mM AA (1 mL). The reaction mixture was incubated in an oven at 95 °C for 2 h. Large Au NSs and Au CNCs were prepared by following a reported method.[36] Au NCs were prepared through a previously reported method with 65 μL of the Au NP seed solution.[37] For the preparation of small Au NSs, 0.1 mL of a 10-fold diluted Au NP seed solution was added to a mixture of 100 mM CTAC (20 mL), 5 mM $HAuCl_4{\cdot}3H_2O$ (2 mL), and 300 mM AA (1 mL). The reaction mixture was incubated at room temperature for 12 h. Au bipyramids were synthesized by following a reported procedure.[38] To prepare Au@Ag core–shell NOs, Au NOs were prepared by following a reported method with 80 μL of the Au NP seed solution.[39] Then, 10 mL of CTAC (30 mM), 10 mL of Au NO solution, 65 μL of $AgNO_3$ (10 mM), and 100 μL of AA (100 mM) were mixed under vigorous stirring. The resulting solution was placed in an oven at 65 °C for 3.5 h.

Preparation of 1D Au NP chains

To prepare 1D Au NP chains, 20 mL of an Au NP solution was concentrated to 0.5 mL by centrifugation at 8000 rpm for 20 min twice with a refrigerated large-capacity centrifuge (Combi-514 R, Hanil Science Industrial), and an AAO template (*ca.* 1.0 × 1.5 cm^2) was treated with H_2O_2 for 1 h, followed by rinsing with copious amounts of water. The H_2O_2-treated AAO template was placed on a Buchner funnel (5 cm^2) equipped with a vacuum filtration system. Approximately 60–80 μL of the concentrated NP solution was loaded into the AAO template under vacuum, and the top of the Buchner funnel was covered with a Petri dish. Then, the AAO template was tilted side to side to facilitate the packing of Au NPs into the AAO pores. Upon drying, the NP-loaded template was briefly sonicated and rinsed with water. These loading and cleaning steps were repeated at least 2 times to fully infiltrate the NPs into the pores of the AAO template, which could be verified by the uniform color distribution on the AAO surface. Before removing the AAO template, the NP-loaded AAO was treated with 1.5 mL of 0.25 wt% DAAB in ethanol overnight, rinsed with ethanol, and completely dried in air. The resulting NP-loaded AAO was placed in an Eppendorf tube containing an aqueous solution of CTAC (0.75 mL, 100 mM). Then the tube was placed on an orbital platform shaker (Heidolph Unimax 2010) and shaken at 100 rpm for 30 min. 0.75 mL of 1 M phosphoric acid was then added to the tube, and the mixture was shaken for an additional 1 h. The AAO was taken out and placed in a new tube containing 1.0 mL of the CTAC solution, followed by brief sonication to collect the 1D NP chains. The isolation of the NP chains from the template was easily monitored by distinctive color changes. After the removal of the template, the tube was placed in a rack without agitation to induce the precipitation of the NP chains. The precipitate was re-suspended in fresh water (0.5 mL).

Preparation of Au NO–AuAg peapod nanostructures

First, the prepared colloidal solution of Au@Ag NO 1D chains was centrifuged at 5000 rpm for 10 min and redispersed in 10 mL of CTAC (10 mM). This step was repeated twice, and the final precipitate was redispersed in 7.5 mL of water. The resulting solution was diluted with water until the absorbance at 566 nm was adjusted to 0.270. Then, to overgrow Ag on the Au@Ag NO 1D chains, 7.5 mL of the prepared Au@Ag NO 1D chain solution, 30 mM CTAC (7.5 mL), 10 mM $AgNO_3$ (65 μL), and 100 mM AA (100 μL) were mixed and incubated in an oven at 65 °C for 3.5 h. For the galvanic replacement reaction, 0.8 mL of CTAC solution (10 mM) was pre-heated to 100 °C in an oil bath. Then, 13.5 mL of the Ag-overgrown Au@Ag NO 1D chain solution was added to the solution, and the resultant

mixture was stirred in the oil bath for 5 min (100 °C, 450 rpm). 40 μL of $HAuCl_4$ (0.5 mM) was then added to the mixture, and the mixture was stirred for 10 min. The resultant mixture was then centrifuged at 5000 rpm, and the product was redispersed in 1.4 mL of water. This galvanic replacement step was repeated with 375 μL of $HAuCl_4$ solution (0.5 mM) to form well-defined AuAg shells. After the mixture was removed from the oil bath, 27 μL of ammonia solution (10-fold diluted in water) was added to the mixture, and the mixture was stirred at 450 rpm for 15 min. To remove the residual Ag, the mixture was centrifuged at 5000 rpm for 10 min, and the product was redispersed in 600 μL of CTAC (50 mM). To this solution, 50 μL of H_2O_2 solution was added, and the resultant solution was sonicated and then left undisturbed for 2 h. The final product was washed twice with an aqueous solution of CTAC (100 mM).

Characterization

SEM images were obtained using a field-emission scanning electron microscope (Philips Model XL30 S FEG). TEM images were collected using a field-emission transmission electron microscope (Tecnai F20, FEI) operated at 200 kV. HAADF–STEM and EDS measurements were performed with a field-emission transmission electron microscope (Talos F200X, Thermo Fisher) operated at 200 kV. UV-vis-NIR extinction spectra were recorded using a Shimadzu UV-3600 UV-vis-NIR spectrometer. The wettability of the AAO surface was evaluated using a contact angle analyzer (Phoenix 300, S.E.O. Co., Ltd) with a water droplet at room temperature.

FDTD simulations

FDTD simulations were performed using the Ansys Lumerical FDTD simulation package. The computational domain was filled with water (refractive index = 1.33), and the mesh size was set to 0.5 nm. The dielectric constants of Au as a function of frequency have been taken from the literature.[40] For the FDTD simulations of the model Au NO–AuAg peapod nanostructure, the Au : Ag atomic ratio (40 : 60) of the shell part was derived from EDS elemental analysis, and its dielectric constants have been taken from the literature.[41] The incident light was a plane wave with a specific wavelength and was propagated under perfectly matched layer (PML) boundary conditions.

Single-particle SERS measurements

A Si wafer was sequentially rinsed with water, acetone, and ethanol (10 min each), and then used as a substrate for single-particle SERS measurements. An Au NO–AuAg peapod nanostructure dispersion was diluted 10-fold with water, and 0.2 mL of the diluted solution was drop-cast on the Si wafer and spin-coated using an ACE-200 spin coater (Dong Ah Trade Corp.). After spin coating, individual nanostructures were located by SEM, and SERS spectra were acquired from the SEM-identified structures. Prior to SERS measurements, the substrate was immersed in an ethanol solution of 4-MBT (5 mM) for 24 h at 85 °C and then rinsed with ethanol. SERS spectra were collected using an Acton SP2300 spectrometer (Princeton Instruments) with a 633 nm He–Ne laser, which was focused on the sample through a 100× objective lens (numerical aperture = 0.9). The laser power was set to 18.75 mW to minimize dye decomposition. Each spectrum was obtained with 1 s integration and 10 accumulations.

Author contributions

S. W. Han conceived the idea and directed the study. J.-H. Kim carried out the synthesis of the NP 1D chains and obtained the characterization data. J. Y. Jung contributed to the synthesis of the Au NO–AuAg peapod nanostructures. Y. Kim carried out the FDTD simulations. U. J. Pyo contributed to the preparation of the figures and supported the experiments. Y. Han synthesized the Au bipyramids. S. Lee and J. W. Hong contributed to the design of the experiments. D. H. Wi contributed to the data interpretation. J.-H. Kim, D. H. Wi, and S. W. Han wrote the manuscript. All authors discussed the results and commented on the manuscript.

Conflicts of interest

There are no conflicts to declare.

Data availability

The data supporting the findings of this study are available within the article and the Supplementary information (SI).

SI includes additional experimental results and supporting figures: SEM images of an AAO template; SEM images of NP building blocks; distributions of the number of particles per chain for Au NS, NC, and CNC 1D chains; SEM images and particle number distributions of Au NS 1D chains prepared without the DAAB treatment; microscopy images and UV-vis-NIR extinction spectra of large Au NS 1D chains; simulated extinction spectra of model Au NS 1D zigzag chains with varying chain lengths; UV-vis-NIR extinction spectra, simulated electric field intensity distributions, and single-particle SERS data of Au NO–AuAg peapod nanostructures. See DOI: https://doi.org/10.1039/d6nr00946h.

Acknowledgements

This work was supported by the National Research Foundation of Korea (NRF) grant funded by the Korean government (MSIT) (No. RS-2024-00350471). This work was also supported by the KAIST KC30 project. D. H. W. acknowledges the support from the research fund of Chungnam National University.

References

1 S. Lee, K. Sim, S. Y. Moon, J. Choi, Y. Jeon, J.-M. Nam and S.-J. Park, *Adv. Mater.*, 2021, **33**, 2007668.
2 Y. Wy, H. Jung, J. W. Hong and S. W. Han, *Acc. Chem. Res.*, 2022, **55**, 831–843.
3 Y. Whang, Y. Kwon, H. Ahn, J. W. Hong and S. W. Han, *Chem. Phys. Rev.*, 2023, **4**, 021312.
4 H. Duan, Z. Jia, M. Liaqat, M. D. Mellor, H. Tan, M.-P. Nieh, Y. Lin, S. Link, C. F. Landes and J. He, *ACS Nano*, 2023, **17**, 12788–12797.
5 Z. Yin, Y. Wang, C. Song, L. Zheng, N. Ma, X. Liu, S. Li, L. Lin, M. Li, Y. Xu, W. Li, G. Hu, Z. Fang and D. Ma, *J. Am. Chem. Soc.*, 2018, **140**, 864–867.
6 X. Zhang, L. Lv, L. Ji, G. Guo, L. Liu, D. Han, B. Wang, Y. Tu, J. Hu, D. Yang and A. Dong, *J. Am. Chem. Soc.*, 2016, **138**, 3290–3293.
7 S. J. Barrow, A. M. Funston, D. E. Gómez, T. J. Davis and P. Mulvaney, *Nano Lett.*, 2011, **11**, 4180–4187.
8 Z. Nie, D. Fava, E. Kumacheva, S. Zou, G. C. Walker and M. Rubinstein, *Nat. Mater.*, 2007, **6**, 609–614.
9 A. Klinkova, H. Thérien-Aubin, A. Ahmed, D. Nykypanchuk, R. M. Choueiri, B. Gagnon, A. Muntyanu, O. Gang, G. C. Walker and E. Kumacheva, *Nano Lett.*, 2014, **14**, 6314–6321.
10 B. Gao, G. Arya and A. R. Tao, *Nat. Nanotechnol.*, 2012, **7**, 433–437.
11 V. P. Nguyen, W. Qian, Y. Li, B. Liu, M. Aaberg, J. Henry, W. Zhang, X. Wang and Y. M. Paulus, *Nat. Commun.*, 2021, **12**, 34.
12 Z. Nie, A. Petukhova and E. Kumacheva, *Nat. Nanotechnol.*, 2010, **5**, 15–25.
13 T. Chen, H. Wang, G. Chen, Y. Wang, Y. Feng, W. S. Teo, T. Wu and H. Chen, *ACS Nano*, 2010, **4**, 3087–3094.
14 F. Zhang, R. Liu, Y. Wei, J. Wei and Z. Yang, *J. Am. Chem. Soc.*, 2021, **143**, 11662–11669.
15 A. M. Steiner, M. Mayer, M. Seuss, S. Nikolov, K. D. Harris, A. Alexeev, C. Kuttner, T. A. F. König and A. Fery, *ACS Nano*, 2017, **11**, 8871–8880.
16 E. Miele, S. Raj, Z. Baraissov, P. Král and U. Mirsaidov, *Adv. Mater.*, 2017, **29**, 1702682.
17 V. T. Cong, E.-O. Ganbold, J. K. Saha, J. Jang, J. Min, J. Choo, S. Kim, N. W. Song, S. J. Son, S. B. Lee and S.-W. Joo, *J. Am. Chem. Soc.*, 2014, **136**, 3833–3841.
18 R. Liang, J. Xu, R. Deng, K. Wang, S. Liu, J. Li and J. Zhu, *ACS Macro Lett.*, 2014, **3**, 486–490.
19 K. Wang, S.-M. Jin, J. Xu, R. Liang, K. Shezad, Z. Xue, X. Xie, E. Lee and J. Zhu, *ACS Nano*, 2016, **10**, 4954–4960.
20 V. T. Cong, N. H. Ly, S. J. Son, J. Min and S.-W. Joo, *Chem. Commun.*, 2017, **53**, 5009–5012.
21 Z. Fang, J. Dong, Y. Fan, C. Li, Q. Han, C. Zhang, L. Zhu, X. Yan, J. Qi and W. Gao, *ACS Omega*, 2025, **10**, 18764–18774.
22 M. N. O'Brien, M. R. Jones, K. A. Brown and C. A. Mirkin, *J. Am. Chem. Soc.*, 2014, **136**, 7603–7606.
23 A. Carone, S. Emilsson, P. Mariani, A. Désert and S. Parola, *Nanoscale Adv.*, 2023, **5**, 2017–2026.
24 H. Jung, J. Y. Jung, S. Kang, Y. Kim, D. H. Wi, H. C. Kim, Y. Kim, J. W. Hong and S. W. Han, *Nano Lett.*, 2026, **26**, 126–133.
25 Z.-B. Liu, Y. Zhang, J.-J. Yu, A. F.-T. Mak, Y. Li and M. Yang, *Sens. Actuators, B*, 2010, **143**, 776–783.
26 A. M. M. Jani, D. Losic and N. H. Voelcker, *Prog. Mater. Sci.*, 2013, **58**, 636–704.
27 L. Guerrini, I. Izquierdo-Lorenzo, R. Rodriguez-Oliveros, J. A. Sanchez-Gil, S. Sanchez-Cortes, J. V. Garcia-Ramos and C. Domingo, *Plasmonics*, 2010, **5**, 273–286.
28 L. O. Herrmann, V. K. Valev, C. Tserkezis, J. S. Barnard, S. Kasera, O. A. Scherman, J. Aizpurua and J. J. Baumberg, *Nat. Commun.*, 2014, **5**, 4568.
29 A. Teulle, M. Bosman, C. Girard, K. L. Gurunatha, M. Li, S. Mann and E. Dujardin, *Nat. Mater.*, 2015, **14**, 87–94.
30 L. S. Slaughter, B. A. Willingham, W.-S. Chang, M. H. Chester, N. Ogden and S. Link, *Nano Lett.*, 2012, **12**, 3967–3972.
31 C. Hanske, M. Tebbe, C. Kuttner, V. Bieber, V. V. Tsukruk, M. Chanana, T. A. F. König and A. Fery, *Nano Lett.*, 2014, **14**, 6863–6871.
32 J. Zhang, M. R. Langille, M. L. Personick, K. Zhang, S. Li and C. A. Mirkin, *J. Am. Chem. Soc.*, 2010, **132**, 14012–14014.
33 M. Rycenga, M. R. Langille, M. L. Personick, T. Ozel and C. A. Mirkin, *Nano Lett.*, 2012, **12**, 6218–6222.
34 P. Matteini, M. de Angelis, L. Ulivi, S. Centi and R. Pini, *Nanoscale*, 2015, **7**, 3474–3480.
35 X. Wang, G. Li, Y. Ding and S. Sun, *RSC Adv.*, 2014, **4**, 30375–30383.
36 D. H. Wi, S. Y. Park, S. Lee, J. Sung, J. W. Hong and S. W. Han, *J. Mater. Chem. A*, 2018, **6**, 13225–13235.
37 H.-L. Wu, C.-H. Kuo and M. H. Huang, *Langmuir*, 2010, **26**, 12307–12313.
38 S. Y. Lee, P. V. Tsalu, G. W. Kim, M. J. Seo, J. W. Hong and J. W. Ha, *Nano Lett.*, 2019, **19**, 2568–2574.
39 P.-J. Chung, L.-M. Lyu and M. H. Huang, *Chem. – Eur. J.*, 2011, **17**, 9746–9752.
40 W. M. Haynes, *CRC Handbook of Chemistry and Physics*, CRC Press, Boca Raton, FL, 95th edn, 2014.
41 D. Rioux, S. Vallières, S. Besner, P. Muñoz, E. Mazur and M. Meunier, *Adv. Opt. Mater.*, 2014, **2**, 176–182.